Geophysical Research Letters

RESEARCH LETTER
10.1029/2020GL089883

Swell Modulation on Wind Stress in the Constant Flux Layer

Sheng Chen[1,2,3], Fangli Qiao[1,2,3], Jun A. Zhang[4], Hongyu Ma[1], Yuhuan Xue[1], and Siyu Chen[1]

[1]First Institute of Oceanography, Ministry of Natural Resources, Qingdao, China, [2]Laboratory for Regional Oceanography and Numerical Modeling, Qingdao National Laboratory for Marine Science and Technology, Qingdao, China, [3]Key Laboratory of Marine Sciences and Numerical Modeling, Ministry of Natural Resources, Qingdao, China, [4]NOAA's Atlantic Oceanographic and Meteorological Laboratory, University of Miami, Miami, FL, USA

Abstract The impact of swell on wind stress is investigated through direct three-layer flux measurements taken by a fixed tower in the marine atmospheric boundary layer. Observations confirm that the assumption of constant momentum flux layer is valid under swell-dominated conditions around the reference height of 10 m. The swell can modulate the total wind stress to be less than the turbulent stress derived from the first-order closure method, and the extent of this modulation decreases with height. The critical layer that represents the top of the layer affected by stronger swells is estimated to reach 45-m altitude, and the depth of this layer decreases as the swells weaken and the wind speed increases. Furthermore, a simple swell correction scheme for the total stress calculation is developed, showing good performance against observations.

Plain Language Summary The swell plays a vital role in the modulation of wind stress and has a remarkable influence on the structure of the marine atmospheric boundary layer (MABL). Investigation of the swell impact on wind stress is thus important for understanding the complex air-sea interaction and for improving ocean-atmosphere coupled models. The study investigates the effect of swell on the wind stress in the surface layer using direct flux and wave observations. For the first time, observations confirm that the surface layer satisfies the constant flux layer assumption under swell conditions, and the degree of swell influence on the wind stress decreases with height. The critical height scale that represents the top of layer that has the swell effect may be larger than 45 m, which depends on the wind speed and wave age. A simple scheme is developed to consider the swell effect in total flux calculation. The predicted wind stress by this scheme shows a good agreement with the measured wind stress.

Key Points:
- Multilevel momentum flux measurements confirm the assumption of constant flux layer at around 10 m above sea surface in swell conditions
- Swell impact on the wind stress decreases with height, and an observation-based scheme is developed to account for the swell effect
- The height of the critical layer affected by stronger swells is predicted to reach 45 m, and this height decreases with the wind speeds

Supporting Information:
- Supporting Information S1

Correspondence to:
F. Qiao,
qiaofl@fio.org.cn

Citation:
Chen, S., Qiao, F., Zhang, J. A., Ma, H., Xue, Y., & Chen, S. (2020). Swell modulation on wind stress in the constant flux layer. *Geophysical Research Letters*, *47*, e2020GL089883. https://doi.org/10.1029/2020GL089883

Received 15 JUL 2020
Accepted 12 OCT 2020
Accepted article online 17 OCT 2020

1. Introduction

Over the ocean, surface waves play a crucial role in the determination of the wind stress in the marine atmospheric boundary layer (MABL), which has been widely explored through numerous observations (Grachev et al., 2003; Högström et al., 2015; Smedman et al., 2009) and numerical studies (Babanin et al., 2018; Janssen, 1989; Jiang et al., 2016). Mechanisms for wind stress modulation have two forms, wind-sea and swell, and their impacts on wind stress are fundamentally different (Chen et al., 2019; Hanley & Belcher, 2008). Wind-seas propagating slower than winds decelerate the overlying airflow, which causes an increase in the wind stress, while following-wind swells traveling faster than winds accelerate the overlying airflow, which induces a decrease in the wind stress.

Swells are the most common over the ocean, which can strongly modulate atmospheric turbulence and affect the wind stress. Högström et al. (2015) observed prominent peak at swell frequency in the turbulent velocity co-spectra at a height above 10 m in the MABL. Additionally, Chen et al. (2020) reported that this spectral peak can induce a sharp variation in the co-spectral Ogive curves at a height up to 17 m above the sea surface. Both studies provided observational evidence for the modulation of wind stress by swells. Other recent studies have shown that swells can reduce the wind stress through the form of swell-induced negative stress (Hanley & Belcher, 2008; Wu et al., 2017). When the swells are strong enough, an upward momentum flux from ocean to atmosphere is generated and a wind jet is seen in

the bottom of MABL, as documented by field observations and numerical simulations (Nilsson et al., 2012; Smedman et al., 2009).

Chen et al. (2019) showed that swells can influence the wind stress up to 26-m height above the sea surface through field observations. Moreover, it is predicted by a one-dimensional boundary layer model that swells can affect the MABL structure (Hanley & Belcher, 2008; Song et al., 2015). However, the actual height of the critical layer with the swell impact is difficult to be determined. Previous MABL models were generally developed based on the assumption of constant flux layer to simulate vertical wind profiles and wave-driven wind speed under swell conditions (Semedo et al., 2009; Zou et al., 2018). The assumption of constant flux layer is that the total wind stress τ does not vary with height z in the near-surface MABL:

$$\partial\tau/\partial z = 0 \tag{1}$$

here, $\tau = \tau_{turb} + \tau_{wave} + \tau_{visc} = u_*^2$. Note that the viscous component τ_{visc} can be neglected because it is nonzero only close to the surface; u_* is the friction velocity. τ_{turb} is the turbulent stress, which can be parameterized according to the first-order closure method:

$$\tau_{turb} = K_m \partial U/\partial z \tag{2}$$

here, K_m is the turbulent eddy viscosity and can be approximated through $K_m = \kappa z u_*$; κ=0.4 is the von Kármán constant. The τ_{wave} is the wave-induced stress, which is assumed to decay exponentially with height (Wu et al., 2017):

$$\tau_{wave} = \tau_{wave0}\exp(-Gkz) \tag{3}$$

here τ_{wave0} is the wave-induced stress at the sea surface, and $\tau_{wave0} = \tau - \tau_{turb0}$, where τ_{turb0} is the surface turbulent stress; G is the decay coefficient; k is the peak wavenumber of surface wave, which can be calculated by the dispersion relation $(2\pi/T)^2 = gk\tanh(kh)$; here, T is the peak period, h is the water depth, and g is the acceleration of gravity. Combining Equations 1–3, the wind speed as a function of z is derived:

$$U(z) = \frac{u_*}{\kappa}\ln\frac{z}{z_0} - \frac{\tau_{wave0}}{\kappa u_*}\int_{z_0}^{z}\frac{e^{-Gkz}}{z}dz \tag{4}$$

here, $z_0 = 0.011\frac{u_*^2}{g} + 0.11\frac{\upsilon}{u_*}$ is the aerodynamic roughness length. Note that Chen et al. (2020) showed the direct evidence that the observed stress contains the swell-induced component τ_{wave}, although Voermans et al. (2019) revealed that their observed stress by eddy covariance system (ECS) is the turbulent component.

Danard (1981) estimated that the height of the constant flux layer is approximately 10 m over the water surface. Notably, 10 m is the typical surface layer height that is used in the parameterization of wind stress or drag coefficient in the ocean, climate, and wave models (Babanin & Mcconochie, 2013), as well as in the widely used COARE algorithm for flux calculations. However, Smedman et al. (2009) demonstrated that the stress magnitude decreases significantly with height near the sea surface due to the swell impact based on multilevel tower observations. Mahrt et al. (2018) also observed a substantial decrease of the stress magnitude with height under swell conditions. They pointed out that the nonstationarity of the wind or the shallow MABL may be responsible for the large stress divergence.

The purpose of this study is to investigate whether the constant momentum flux assumption is always invalid in the MABL when swell is dominant and, based on this, to study the swell impact on wind stress. We also aim to quantify the swell effect on the total wind stress and how this effect varies with height and wind speed using observations. This study is organized as follows. The observational data and analysis method are described in section 2. Results and discussions are presented in section 3. A simple correction of swell effect for the estimated wind stress is proposed and presented in this section. Finally, conclusions are summarized in section 4.

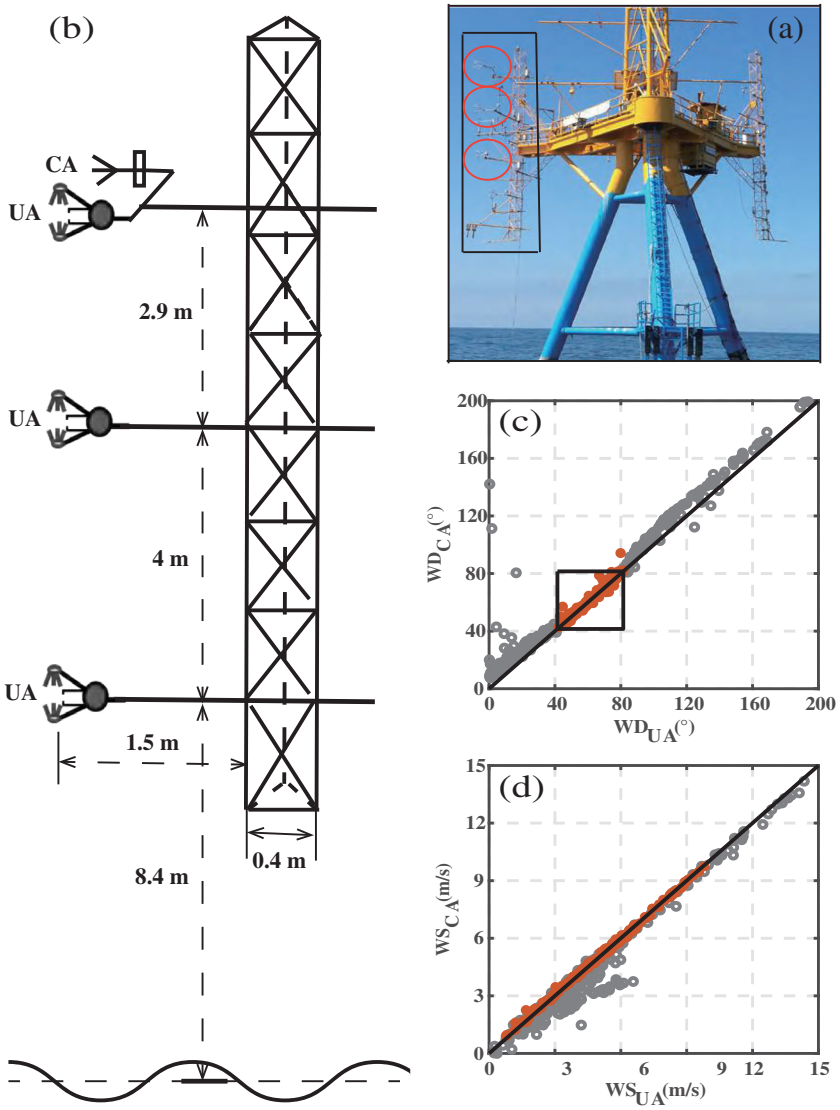

Figure 1. The BHOT in the northern SCS (a). The instrument in the red circle is used. The auxiliary tower used in this study is shown in the black square (a) and its sketch is shown in (b). The instruments of the three-layer flux measurements are shown in (b). CA and UA represent the conventional and ultrasonic anemometers, respectively. The comparisons of wind direction and wind speed observed by UA and CA are presented in (c) and (d). The black square in (c) means the wind direction is between 41° and 81°. The red dots in (c) and (d) correspond to measured values in the black square in (c).

2. Data Collection and Analysis Method

The data used in this study was collected by a fixed observation system, BoHe observation tower (BHOT), over the coastal regions in the northern South China Sea (SCS) as shown in Figure 1a. The mean water depth is approximately 16 m at this tower (21°26.5′N, 111°23.5′E). This BHOT is approximately 6.5 km from the coastline and consists of a main tower and two auxiliary towers. Our ECSs were mounted at three levels on the northeast auxiliary tower from 17 March to 14 May 2018. This auxiliary tower with a diameter of 0.4 m is approximately 6 m away from the main tower. The ECSs were mounted 1.5 m away from the side of the auxiliary tower. This distance is enough to minimize the flow distortion caused by the tower (Chen et al., 2018; Gill et al., 1967). The three levels of ECSs were 8.4, 12.4, and 15.3 m, respectively, above the sea surface (Figure 1b).

Each ECS consists of a three-dimensional ultrasonic anemometer (UA) with orientation of ~61° north by east, an infrared gas analyzer, and high-frequency temperature and humidity sensors, which can

continuously collect atmospheric turbulence data with a sampling frequency of 10 Hz. These data can be used to calculate air-sea fluxes. Additionally, a propeller type conventional anemometer (CA) was installed at a distance of 1 m on the right side of the upper ECS to observe the mean wind speed and direction, which can be used to validate the mean wind speed and direction from the UA. During the observational periods, a bottom-supported wave buoy was deployed to simultaneously measure surface waves near the tower.

We focus on the air-sea momentum flux measured by the UA in this study. Based on the eddy covariance method, the wind stress can be calculated directly through:

$$\tau = -\overline{U'w'} = u_*^2 \tag{5}$$

here, U' and $w'$are the horizontal and vertical velocity fluctuations (Babanin & Makin, 2008), $u_* = \sqrt{-\overline{U'w'}}$. The Reynolds average time of 1 h was chosen. Note that the nonstationary motions were removed from 1-h turbulence data before the calculation of the covariance following the method as in Chen et al. (2018), to guarantee the stationarity and avoid the possible data contamination.

Additionally, we compared the wind directions measured by the upper UA and CA for further quality control. The wind direction and speed measured by the UA compared to those measured by the CA generally fall in the 1:1 line (Figures 1c and 1d). The direction and speed measured by UA within ±20° of the UA orientation match the best, shown by the red dots in Figures 1c and 1d. Therefore, for flux calculations, the data with wind direction between 41° and 81° were selected.

After data quality control, 463 flux runs are obtained, and the wind speeds vary from low to moderate, mostly below 9 m/s (Figure S1a in the supporting information), which further minimize the potential flux contamination caused by the tower motion. During the period of interest, swells always occur and travel in the southeast direction with an average of approximately 120° because of the northwest coastline (Chen et al., 2018, 2020, see their Figure 2). Besides, the wave age $\beta = C_p/U\cos\theta$ is mostly greater than 1.2 (Figure S1b), where C_p is the peak wave phase speed and θ is the wave off-wind angle. The swell significant wave height H_s^{swell} is generally higher than that of wind-sea $H_s^{windsea}$ (Figure S1c). Both results suggest that the swells dominate the wave field (Högström et al., 2015). The simultaneous surface wave and flux data are analyzed to investigate the impact of swell on the wind stress.

3. Results and Discussions

3.1. Constant Flux Layer

Because the wind stress at low wind speeds is very small, we present the friction velocity u_* rather than the stress. The friction velocities at three levels are compared in Figure 2, showing a significant agreement among all levels. The bias between $u_{*middle}$ and u_{*lower} and that between u_{*upper} and u_{*lower} are close to 0. This result suggests that the assumption of constant flux layer at around 10 m is validated in our study. The vertical gradient of the wind stress, $\partial\tau/\partial z$, is on the order of 10^{-4} m/s^2, and the averaged stress divergence approaches 0, which further confirm this constant flux layer. Of note, Babanin and Makin (2008) argued that the constant flux concept is impossibly satisfied at low wind speeds ($U_{10} < 4$ m/s) and the constant flux layer height is less than 10 m in this condition following Komen (1994). Their conclusion was inferred from a simple comparison between the friction velocity calculated through the logarithmic profile method and that directly obtained from the limited single level ultrasonic measurement. However, our three-layer momentum flux measurements avoid this limitation and show that the wind stress around 10 m satisfies the condition of constant flux, even at low wind speeds (Figure 2). Again, this height (10 m) is similar to the theoretical surface layer height proposed by Danard (1981).

Our result indicates that the total wind stress does not vary with height even in the presence of swells, which differs significantly from that of Mahrt et al. (2018) and Smedman et al. (2009) who showed large stress divergence due to swells. As the stress divergence may be caused by factors such as the nonstationarity of the wind and the thin boundary layer (Mahrt et al., 2018), the marine condition in our study is likely very different from that in these two studies.

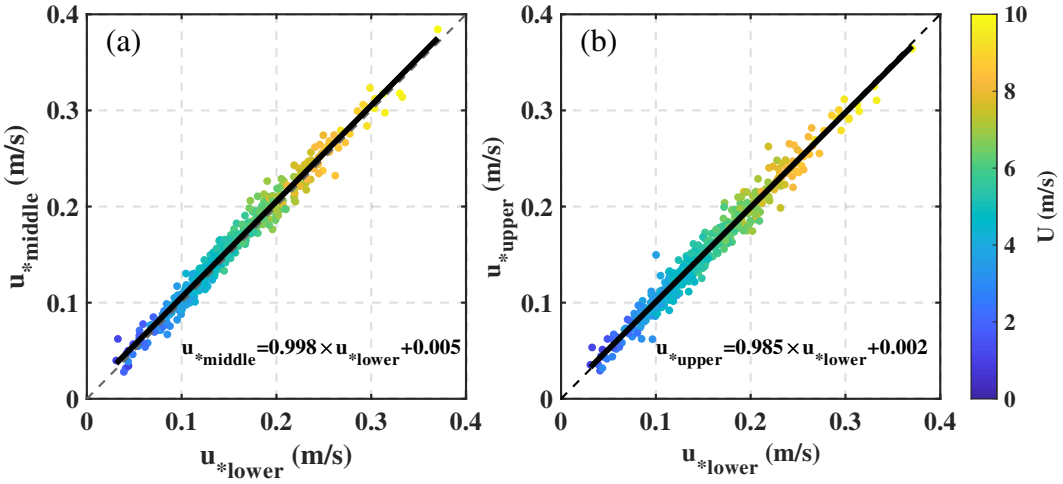

Figure 2. Comparison of friction velocity between the middle $u_{*middle}$ and lower u_{*lower} levels (a) and between upper u_{*upper} and lower u_{*lower} levels (b). The dashed and slid lines represent the 1:1 scale line and the best fitted line between each other, respectively. U represents the wind speed at the height of 8.4 m.

3.2. Swell Impact on Wind Stress

According to classic turbulence theory (Tennekes & Lumley, 1972), the mean velocity profile follows the log-law when the measurement is taken sufficiently away from wall or boundary where the wind is independent of the types of the stresses. Similarly, when the wave-induced stress is negligible (i.e., $\tau_{wave} = 0$) in the MABL, $\tau = \tau_{turb}$, and consequently, $u_* = u_{*turb}$, here, u_{*turb} is the turbulent friction velocity, Equation 4 is reduced to

$$U(z) = \frac{u_*}{\kappa}\ln\frac{z}{z_0} \tag{6}$$

For comparison purposes, u_* in the absence of wave-induced stress is expressed as u_{*turb} hereafter. Note that the wind stress calculated based on the COARE algorithm is consistent with that estimated using Equation 6 because the wave effect is not considered (Fairall et al., 2003). We can estimate the turbulent stress using the COARE algorithm and observed mean wind speeds, although the wave-induced stress is not negligible at the instrument measurement height in our study. The difference between the estimated turbulent stress and directly measured total stress is thus equivalent to the wave-induced stress.

As mentioned earlier, quantifying the swell impact on the wind stress is the focus of this study. Data with wind speeds at lower layer greater than 9 m/s are excluded due to quality control and a total of 448 sets of flux runs are obtained. For the total wind stress, we use the observations at the height of 8.4 m based on the premise condition of constant flux layer. Comparison between the turbulent stress estimated based on the COARE algorithm and the observed stress are shown in Figure 3, where u_{*obs} is the observed friction velocity. It is evident from Figure 3a that u_{*turb} deviates significantly from u_{*obs} at the lower level, with a positive bias of 0.031 m/s. The extent of this deviation decreases with height, but the estimated u_{*turb} is still greater than the actual observation at middle and upper levels (Figures 3b and 3c). It is the swells that cause this deviation of the estimated stress from the observed one. The swells can induce a negative wave-induced stress, $\tau_{wave} < 0$ (Hanley & Belcher, 2008; Semedo et al., 2009), which results in the total wind stress being less than the turbulent stress $\tau < \tau_{turb}$. Besides, the magnitude of swell-induced stress decays exponentially with height (Hristov et al., 2003; Jiang et al., 2016), which causes the turbulent component to approach the total stress as the height increases.

The wave-induced stress can be calculated through the wave spectrum, which has been widely used to correct the turbulent stress to be consistent with the actual total stress (Babanin et al., 2018; Chen et al., 2019; Zou et al., 2018). Here, we apply the same method into our observations and find that this correction is feasible (Figure S2). We develop a simple parameterization to correct the calculated turbulent stress τ_{turb} with

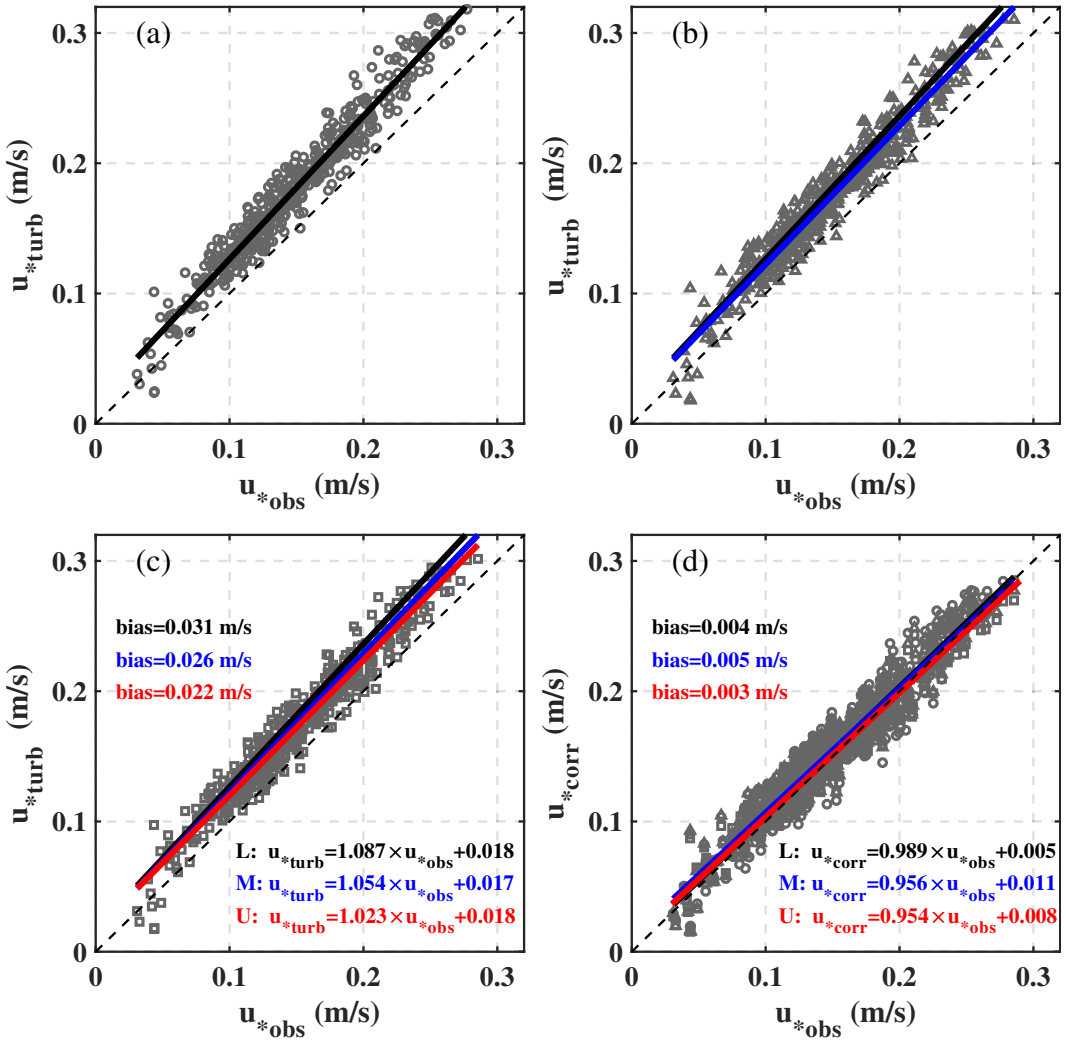

Figure 3. Comparison between the friction velocity u_{*turb} without considering the wave effect (a–c), the corrected friction velocity u_{*corr} (d) and the observed friction velocity u_{*obs} at the height of 8.4 m. Circles in (a) and (d), triangles in (b) and (d), and squares in (c) and (d) represent the observations at the lower, middle, and upper levels, respectively. The dashed black lines in all subplots represent the 1:1 scale line. The black, blue, and red lines show the best fitted lines between the calculated and observed friction velocities for three levels from lower to upper, respectively.

only one wave parameter. According to Equation 3, the magnitude of τ_{wave} can be expressed in terms of the calculated turbulent stress τ_{turb} in the absence of wave effect:

$$|\tau_{wave}| = \alpha\tau_{turb} = \left(\frac{\exp(-Gkz)}{1-\exp(-Gkz)} + A\right)\tau_{turb} \tag{7}$$

where α is a correction factor. Coefficients G and A can be determined using observations. Note that Equation 7 in our study is similar to Equation 20 in Voermans et al. (2019), although they parameterized the wave-induced stress using the significant wave height H_s and the observed turbulent stress. Considering the swell-induced stress is negative, the total stress is formulated as

$$\tau = \tau_{turb} + \tau_{wave} = \tau_{turb} - \alpha\tau_{turb} \tag{8}$$

The coefficients, G and A, can be determined using the observed wind stress at lower and upper levels in our study, and the best fit values are $G = 3$ and $A = 0.2$. This value of coefficient A is equal to that of

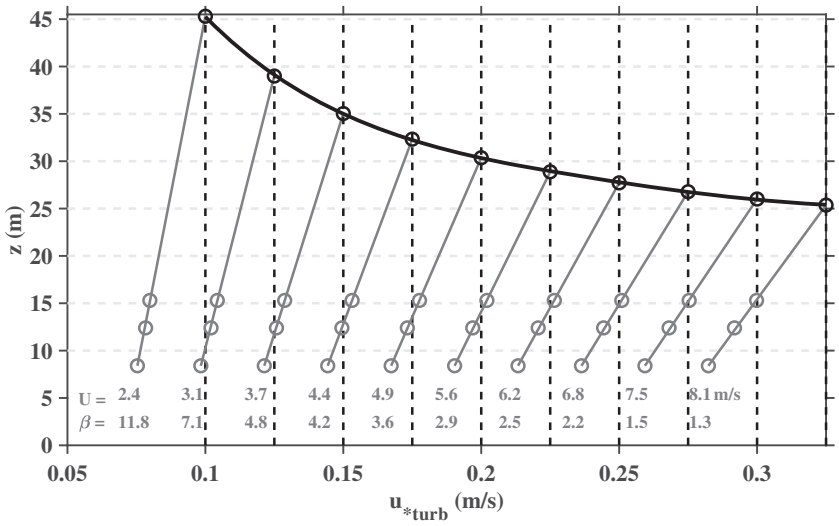

Figure 4. The profiles of friction velocities obtained by means of the best fitted lines in Figure 3c. The gray solid lines represent the fitted lines for three levels and the vertical black dashed lines represent the corresponding friction velocities u_{*turb} in the absence of waves. The black solid line with circles shows the maximum height that swells can affect the wind stress.

Voermans et al. (2019), although they derived A by fitting their observed turbulent stress and H_s. Then, we use the observed wind stress at the middle level to evaluate the robustness of our parameterization of the wave-induced stress. Figure 3d shows the comparison of the corrected friction velocities by our parameterization and the observed ones, showing a good agreement. This result supports that the wind stress corrected by our parameterization (i.e., Equations 7 and 8) with the observation-derived coefficients can be used to estimate the total wind stress at a typical height of 10 m. Furthermore, this parameterization can be used to modify the COARE algorithm and correct the wind stress under following-wind swell conditions.

It should be noted that the swell with off-wind angle less than 90° is the most prevalent in our observations; therefore, α is negative. However, the counter-wind swells can cause increasing wind stress (Donelan et al., 1997), so that the observed stress is greater than the estimated turbulent stress by the COARE algorithm and α should be positive in such conditions. When applying our method for correcting the wave-induced stress in the COARE algorithm, the wind and wave states need to be determined first. Thus, more experiments under different sea states, including counter-wind swell condition, are needed to confirm the form of wave-induced stress for a universal application.

3.3. Critical Layer Height

The extent of swell influence on wind stress decreases with height, which implies that the swell-induced stress will approximately approach zero ($\tau_{wave}\rightarrow 0$) at sufficient level where the total wind stress equals the turbulent stress: $\tau = \tau_{turb}$. The maximum height or the critical layer height below which swells affect the total wind stress can be estimated based on three-layer stress observations. After the turbulent stress is calculated through Equations 2 and 6, the total wind stress at each level can be determined using the corresponding best fit equation shown in Figure 3c. The three-layer friction velocity profiles are displayed in Figure 4. Based on the nearly linear relationship between the friction velocity u_{*turb} and the lower-level wind speed U, the corresponding wind speed U for each profile is determined. The wave age β is also shown in Figure 4. The critical layer height for swells has a minimum value of 25 m based on our observations (Figure 4), and 2% of τ_{wave0} is the cutoff value in Equation 3 at this minimum height.

The critical layer height for swells can reach 45 m or more and decreases with the wind speed. This height scale increases with the wave age (Figure 4), suggesting that the perturbations induced by stronger swells are more likely to be caught at a certain height above the sea surface. Chen et al. (2019) observed swell-induced disturbances in the turbulent velocity spectra at a height of 26 m in the MABL for wind speeds <5 m/s.

Furthermore, Smedman et al. (2009) reported large influence of swells on the wind velocity at 30 m above the sea surface under both cross-wind swell ($|\beta| > 2.8$) and following-wind swell ($|\beta| > 1.8$) conditions. They also showed more pronounced impacts of stronger swells on the wind field than weaker swells. Both are quite similar to our estimation of critical layer height. Additionally, it should be noted that the critical heights derived from the wind stress profiles are similar to those shown in Figure 4.

4. Conclusions

Multilevel observations of momentum fluxes above the sea surface show that the wind stress around the typical surface layer height of 10 m satisfies the assumption of constant flux layer at low to moderate wind speeds. Swells have a significant effect on the wind stress, which act to reduce the total wind stress to be less than the turbulent stress derived from the first-order closure method or the COARE algorithm without considering the wave effect. We found that the swell-induced stress can be used to correct the bias between the turbulent and total stress using a simple correction parameterization based on observations. This parameterization only requires the calculated turbulent stress using the COARE algorithm and the peak wavenumber of surface wave to determine the total wind stress under swell conditions. Furthermore, the swell influence on the wind stress is found to decrease with height, which can be used to estimate the critical layer height affected by swells. We found that the maximum height that swells can affect is expected to reach 45 m, and this critical height decreases with the decreasing wave age and the increasing wind speed. Our results provide the first evidence for the concept of a near constant flux layer with a height of ~10 m, and provide a promising method to determine the critical layer affected by swells. This method along with the wave-induced stress parameterization require further verification through the multilayer flux measurements under different wind conditions and sea state in future studies.

Data Availability Statement

Data supporting this study are available by any users from http://data.fio.org.cn/qiaofl/CS-GRL-2020 website.

Acknowledgments

This research was jointly supported by the National Natural Science Foundation of China under Grants 41821004 and 41776038, Project funded by China Postdoctoral Science Foundation under Grant 2019M662472, and Postdoctoral Applied Research Project of Qingdao. Jun Zhang was supported by NOAA Grant NA14NWS4680028 and National Science Foundation Grant AGS-1822128. The authors are grateful to the platform maintenance personnel from the Guangzhou Institute of Tropical and Marine Meteorology.

References

Babanin, A. V., & Makin, V. K. (2008). Effects of wind trend and gustiness on the sea drag: Lake George study. *Journal of Geophysical Research*, *113*, C02015. https://doi.org/10.1029/2007JC004233

Babanin, A. V., & Mcconochie, J. (2013). *Wind measurements near the surface of waves*. Paper presented at Proceedings of the ASME 2013 32nd International Conference on Ocean, Offshore and Arctic Engineering. Nantes, France.

Babanin, A. V., McConochie, J., & Chalikov, D. (2018). Winds near the surface of waves: Observations and modeling. *Journal of Physical Oceanography*, *48*(5), 1079–1088. https://doi.org/10.1175/JPO-D-17-0009.1

Chen, S., Qiao, F., Huang, C. J., & Zhao, B. (2018). Deviation of wind stress from wind direction under low wind conditions. *Journal of Geophysical Research: Oceans*, *123*, 9357–9368. https://doi.org/10.1029/2018JC014137

Chen, S., Qiao, F., Jiang, W., Guo, J., & Dai, D. (2019). Impact of surface waves on wind stress under low to moderate wind conditions. *Journal of Physical Oceanography*, *49*(8), 2017–2028. https://doi.org/10.1175/JPO-D-18-0266.1

Chen, S., Qiao, F., Xue, Y., Chen, S., & Ma, H. (2020). Directional characteristic of wind stress vector under swell-dominated conditions. *Journal of Geophysical Research: Oceans*, *125*, e2020JC016352. https://doi.org/10.1029/2020JC016352

Danard, M. (1981). A note on estimating the height of the constant flux layer. *Boundary Layer Meteorology*, *20*(3), 397–398. https://doi.org/10.1007/BF00121382

Donelan, M. A., Drennan, W. M., & Katsaros, K. B. (1997). The air-sea momentum flux in conditions of wind sea and swell. *Journal of Physical Oceanography*, *27*(10), 2087–2099. https://doi.org/10.1175/1520-0485(1997)027<2087:TASMFI>2.0.CO;2

Fairall, C. W., Bradley, E. F., Hare, J. E., Grachev, A. A., & Edson, J. B. (2003). Bulk parameterization of air–sea fluxes: Updates and verification for the COARE algorithm. *Journal of Climate*, *16*(4), 571–591. https://doi.org/10.1175/1520-0442(2003)016<0571:bpoasf>2.0.co;2

Gill, G. C., Olsson, L. E., Sela, J., & Suda, M. (1967). Accuracy of wind measurements on towers or stacks. *Bulletin of the American Meteorological Society*, *48*(9), 665–675. https://doi.org/10.1175/1520-0477-48.9.665

Grachev, A. A., Fairall, C. W., Hare, J. E., Edson, J. B., & Miller, S. D. (2003). Wind stress vector over ocean waves. *Journal of Physical Oceanography*, *33*(11), 2408–2429. https://doi.org/10.1175/1520-0485(2003)033<2408:wsvoow>2.0.co;2

Hanley, K. E., & Belcher, S. E. (2008). Wave-driven wind jets in the marine atmospheric boundary layer. *Journal of the Atmospheric Sciences*, *65*(8), 2646–2660. https://doi.org/10.1175/2007jas2562.1

Högström, U., Sahlée, E., Smedman, A. S., Rutgersson, A., Nilsson, E., Kahma, K. K., & Drennan, W. M. (2015). Surface stress over the ocean in swell-dominated conditions during moderate winds. *Journal of the Atmospheric Sciences*, *72*(12), 4777–4795. https://doi.org/10.1175/JAS-D-15-0139.1

Hristov, T. S., Miller, S. D., & Friehe, C. A. (2003). Dynamical coupling of wind and ocean waves through wave-induced air flow. *Nature*, *422*(6927), 55–58. https://doi.org/10.1038/nature01382

Janssen, P. A. E. M. (1989). Wave-induced stress and the drag of air flow over sea waves. *Journal of Physical Oceanography*, *19*(6), 745–754. https://doi.org/10.1175/1520-0485(1989)019<0745:WISATD>2.0.CO;2

Jiang, Q., Sullivan, P., Wang, S., Doyle, J., & Vincent, L. (2016). Impact of swell on air-sea momentum flux and marine boundary layer under low-wind conditions. *Journal of the Atmospheric Sciences*, *73*(7), 2683–2697. https://doi.org/10.1175/JAS-D-15-0200.1

Komen, G. I. (1994). Sea surface winds and atmospheric circulation. In G. I. Komen, et al. (Eds.), *Dynamics and modelling of ocean waves* (pp. 48–60). Cambridge, UK: Cambridge University Press.

Mahrt, L., Miller, S., Hristov, T., & Edson, J. (2018). On estimating the surface wind stress over the sea. *Journal of Physical Oceanography*, *48*(7), 1533–1541. https://doi.org/10.1175/JPO-D-17-0267.1

Nilsson, E. O., Rutgersson, A., Smedman, A. S., & Sullivan, P. (2012). Convective boundary-layer structure in the presence of wind-following swell. *Quarterly Journal of the Royal Meteorological Society*, *138*(667), 1476–1489. https://doi.org/10.1002/qj.1898

Semedo, A., Saetra, Ø., Rutgersson, A., Kahma, K. K., & Pettersson, H. (2009). Wave-induced wind in the marine boundary layer. *Journal of the Atmospheric Sciences*, *66*(8), 2256–2271. https://doi.org/10.1175/2009JAS3018.1

Smedman, A.-S., Högström, U., Sahlée, E., Drennan, W. M., Kaham, K. K., & Pettersson, H. (2009). Observational study of marine atmospheric boundary layer characteristics during swell. *Journal of the Atmospheric Sciences*, *66*(9), 2747–2763. https://doi.org/10.1175/2009JAS2952.1

Song, J., Fan, W., Li, S., & Zhou, M. (2015). Impact of surface waves on the steady near-surface wind profiles over the ocean. *Boundary-Layer Meteorology*, *155*(1), 111–127. https://doi.org/10.1007/s10546-014-9983-6

Tennekes, H., & Lumley, J. L. (1972). *A first course in turbulence*. Massachusetts, US: Massachusetts Institute of Technology Press. https://doi.org/10.7551/mitpress/3014.001.0001

Voermans, J. J., Rapizo, H., Ma, H., Qiao, F., & Babanin, A. V. (2019). Air-sea momentum fluxes during tropical cyclone Olwyn. *Journal of Physical Oceanography*, *49*(6), 1369–1379. https://doi.org/10.1175/JPO-D-18-0261.1

Wu, L., Rutgersson, A., & Nilsson, E. (2017). Atmospheric boundary layer turbulence closure scheme for wind-following swell conditions. *Journal of Atmospheric Sciences*, *74*(7), 2363–2382. https://doi.org/10.1175/JAS-D-16-0308.1

Zou, Z., Zhao, D., Zhang, J., Li, S., Cheng, Y., Lv, H., & Ma, X. (2018). The influence of swell on the atmospheric boundary layer under nonneutral conditions. *Journal of Physical Oceanography*, *48*(4), 925–936. https://doi.org/10.1175/JPO-D-17-0195.1